Composites Communications 25 (2021) 100742

Contents lists available at ScienceDirect

Composites Communications

journal homepage: www.elsevier.com/locate/coco

High strength SiCp/Al–2Cu-1.2Mg-0.6Si composite with weak natural aging hardening

S.Z. Zhu [a,b], D. Wang [a,**], Y.N. Zan [a,b], B.L. Xiao [a,*], Z.Y. Ma [a]

[a] Shi-changxu Innovation Center for Advanced Materials, Institute of Metal Research, Chinese Academy of Sciences, 72 Wenhua Road, Shenyang, 110016, China
[b] School of Materials Science and Engineering, University of Science and Technology of China, 72 Wenhua Road, Shenyang, 110016, China

ARTICLE INFO

Keywords:
Aluminum alloys
Particulate reinforced composites
Natural aging
Artificial aging

ABSTRACT

The typical SiCp/Al–Cu–Mg composites have strong natural aging hardening trend, thus decreasing performance for cold working after quenching. The study developed a SiCp/Al–2Cu-1.2Mg-0.6Si (in wt.%) composite with low natural aging strength and high natural aging ductility. Compared to the typical SiCp/2009Al (Al–4Cu-1.2 Mg, in wt%) composite, the SiCp/Al–2Cu-1.2Mg-0.6Si composite had a 73 MPa decrement in yield strength and an increment in uniform elongation from 8.5% to 10.5% after one-week natural aging due to much fewer Cu, whereas the composite exhibited a 33 MPa increment in yield strength after artificial aging. Due to modification of precipitation by Si, finer and equal quantity (volume fraction) of intragranular precipitates formed after artificial aging in the SiCp/Al–2Cu-1.2Mg-0.6Si composite in comparison with the SiCp/2009Al composite. Therefore, higher yield strength after artificial aging could be achieved although Cu content was much lower. The SiCp/Al–2Cu-1.2Mg-0.6Si composite exhibited great potential for application, thereby enriching the classification of SiCp/Al composites.

1. Introduction

SiC particles reinforced high-strength Al–Cu–Mg alloys are widely used as load-bearing components, such as SiCp/2009Al and SiCp/2024Al composites [1–4]. Compared to unreinforced alloys, SiCp/2009Al and SiCp/2024Al composites have excellent yield strength (YS) after artificial aging (AA) but they are too brittle to plastically form in the AA state. By contrast, during a very short time after solution and quenching treatments, these composites exhibit relatively high ductility and low YS. This short natural aging (NA) stage is the best chance to conduct cold plastic forming, such as quenching distortion correction and stamping. However, SiCp/2009Al and SiCp/2024Al composites have strong NA hardening, leading to fast strength increase and ductility decrease with prolonged NA time [5,6]. Consequently, it is demanded to develop SiCp/Al composites with low NA strength and high NA ductility. Meanwhile, this kind of composite should have enough AA hardening in order to meet service requirements.

In previous studies [7,8], NA hardness in some Al–Mg–Si alloys was reduced by adding vacancy-seizing elements, such as Sn, to inhibit vacancy-assisted solute clustering. The trapped vacancies could be released to form precipitates at about 170 °C, so AA hardness was not impaired. However, it was reported that Sn had negligible effects on NA hardening in the Al-3.9Cu-1.1 Mg (in wt.%) alloy because Cu and Mg could form clusters before vacancies were seized by Sn [9].

This work intended to reduce NA strength and improve NA ductility through weakening solute strengthening and cluster strengthening, which could be achieved by reducing alloying elements that have large atomic size mismatch and shear modulus mismatch with the Al matrix [5,10]. However, the reduction of alloying elements will decrease strength after AA. In order to maintain high AA strength, micro-alloy elements should be added to modify precipitates, such as size or quantity control [11]. Moreover, these micro-alloy elements should have small atomic size mismatch and shear modulus mismatch with the Al matrix, thereby avoiding significant improvement of NA strength.

According to the above strategy, a SiCp/Al–2Cu-1.2Mg-0.6Si (in wt %) composite was designed. Compared to SiCp/2009Al (3.2–4.4 Cu and 1.0–1.6 Mg, Al bal. (in wt.%)) composites, Cu was reduced drastically to weaken solution strengthening and cluster strengthening, and Si was added in a small amount to enhance precipitation strengthening. Effects of Si on AA precipitation behavior in Al–Cu–Mg alloys have been

* Corresponding author.
** Corresponding author.
E-mail addresses: dongwang@imr.ac.cn (D. Wang), blxiao@imr.ac.cn (B.L. Xiao).

https://doi.org/10.1016/j.coco.2021.100742
Received 6 July 2020; Received in revised form 25 March 2021; Accepted 31 March 2021
Available online 9 April 2021

investigated [12–14], but little attention was paid to their composites. For the composites, the influence of Si on the interface reactions between SiCp and the matrix should also be concerned. In addition, previous studies only reported the independent effect of Si [12], whereas this work paid more attention to how Si replenished AA strength loss caused by Cu reduction without significantly increasing NA strength.

In this work, the synergistic effects of Cu reduction and Si addition on microstructures and mechanical properties of the composites were investigated. The aims of this study are: (I) develop composites with low NA strength and high NA ductility but strong AA hardening; (II) elucidate the related microstructural mechanisms responsible for mechanical property changes.

2. Experiments

Three composites reinforced by 17 vol% SiCp were prepared by powder metallurgy technology including powder mixing, hot pressing, hot extruding with an extrusion ratio of 16:1 and solution treatment at temperatures listed in Table 1. The hot pressing temperatures and solution temperatures of the SiCp/2009Al and SiCp/AlCuMg were selected according to our published work [15,16]. For the SiCp/AlCuMgSi, a higher hot pressing temperature was used for densification and a higher solution temperature was used to adequately dissolve Si-containing phases. The nominal sizes of SiCp (99.5 pct. purity) and alloy powders (99.9 pct. purity) were 7 μm and 13 μm, respectively. The nominal composition of matrices is also listed in Table 1. The SiCp/2009Al was prepared to compare to the SiCp/AlCuMgSi to evaluate the strategy. The SiCp/AlCuMg was also fabricated to clarify the role of Si.

NA was conducted at room temperatures. AA was carried out at 170 °C for different time to determine the highest hardness of the SiCp/AlCuMgSi and SiCp/2009Al.The samples that were artificially aged immediately after quenching to the highest hardness were abbreviated as DPA samples. And the samples that were naturally aged for one week then artificially aged to the highest hardness were abbreviated as NPA samples. The SiCp/AlCuMg was artificially aged with the same DPA and NPA processes as the SiCp/AlCuMgSi in order to expound the effect of Si on AA hardening.

Brinell hardness and Vickers hardness were measured using a Testor 1080 hardometer under a load of 250 kg and a FV-700 hardometer under a load of 10 kg, respectively. At least three indentations were made on each sample. Following the ISO 6892–1: 2009, tensile samples with a gauge length of 35 mm were tested under a strain rate of 1×10^{-3} s^{-1} using an Instron 5982 tensile test machine equipped with an extensometer. The tensile axis was parallel to the extrusion direction. Three samples were tested for each aging condition to calculate average values.

Transmission electron microscopy (TEM) characterization was performed on FEI Tecnai F20. Bright-field (BF) and high-resolution TEM (HRTEM) images were acquired with the electron beam parallel to the $<001>_{Al}$ zone axis. All TEM foil samples were dimpled and ion-milled at about −70 °C. Thermodynamic calculation was conducted using the Thermo-Calc software based on the TT Al-Alloys Database v8.1 to further elucidate the precipitation behavior.

Table 1
Sample designations, nominal composition (Al, Bal.) of matrices and manufacture temperatures of three composites.

Designations	Composition, wt%				Manufacture temperatures, °C		
	Mg	Si	Cu	Total	Hot pressing	Extrusion	Solution
SiCp/AlCuMgSi	1.2	0.6	2.0	3.8	600	450	540
SiCp/2009Al	1.2	/	4.0	5.2	580	450	500
SiCp/AlCuMg	1.2	/	2.0	3.2	580	450	500

3. Results

3.1. Mechanical properties

During NA, the SiCp/AlCuMgSi showed much lower hardness than the SiCp/2009Al, and slightly higher hardness than the SiCp/AlCuMg, indicating that the reduction of Cu significantly reduced NA hardness but the addition of Si slightly increased it (Fig. 1(a)). Compared to the SiCp/2009Al, the SiCp/AlCuMgSi had a 73 MPa reduction in YS and an increment in uniform elongation from 8.5% to 10.5% after one-week NA (Fig. 1(b)).

The SiCp/AlCuMgSi and the SiCp/2009Al attained the DPA state after AA for 8 h and 12 h, respectively (Fig. 1(c)). In the DPA state, the SiCp/AlCuMgSi had the YS of 460 MPa and the ultimate tensile strength of 555 MPa, which were 33 and 25 MPa higher than those of the SiCp/2009Al, respectively (Fig. 1(d)). The SiCp/AlCuMg exhibited the lowest DPA strength due to fewer Cu and free of Si. In the NPA state, the SiCp/AlCuMgSi still had the highest strength among the three composites (Fig. 1(e)).

3.2. Intragranular precipitates

Fig. 2(a–c) shows the BF and corresponding selected area electron diffraction (SAED) images of intragranular precipitates in the DPA composites. All precipitates were elongated along three equivalent $<001>_{Al}$ directions. The SiCp/AlCuMgSi had the finest intragranular precipitates among the three composites, indicating that Si could refine intragranular precipitates.

The HRTEM and corresponding Fast Fourier Transforms (FFT) images of the SiCp/AlCuMgSi in the DPA state are shown in Fig. 2(d–h). The precipitate shown in Fig. 2(d) had a monoclinic structure with the long axis parallel to $<320>_{Al}$ and the short axis parallel to $<310>_{Al}$, so was identified as β'' phases (probably Mg_5Si_6) [17,18]. The precipitate shown in Fig. 2(e) with a disordered narrow rectangular cross-section elongated along $<001>_{Al}$ was in coincidence with L phases (uncertain composition but rich in Cu, Mg and Si) [19]. The precipitate shown in Fig. 2(f) had a length of about 20 nm, and its lattice constant is similar to the Al matrix, so was identified as Guinier-Preston-Bagaryatsky (GPB) zone [12,20].

The precipitate shown in Fig. 2(g) had a body-centered tetragonal crystal structure and the lattice constants of a = 0.404 nm, b = 0.580 nm, which was determined to be θ′ phases [21]. S″ phases were also found (Fig. 2(h)) according to the monoclinic crystal structure [22]. However, the quantity of θ′ and S″ phases was very few.

The equilibrium phase diagrams calculated by Thermo-Calc software are shown in Fig. 3. Compared to those in the Al–Cu–Mg phase diagram, Si promoted the formation of β and Q phases, and changed the position of θ and S phases in the Al–Cu–Mg-0.6 wt%Si phase diagram. Consequently, intragranular precipitates of Al–Mg–Si–Cu (β'' and L phases) and Al–Cu–Mg (GPB zones, θ′ and S″ phases) alloys both existed in the DPA SiCp/AlCuMgSi.

3.3. Intergranular phases

Fig. 4 shows the BF images of intergranular phases (phases at grain boundaries and interfaces between SiCp and the matrix) in the DPA composites. The SiCp/AlCuMgSi (Fig. 4(a) and (d)) had much fewer intergranular phases than the SiCp/2009Al (Fig. 4(b) and (e)) and SiCp/AlCuMg (Fig. 4(c) and (f)), suggesting that Si plays an important role in reducing intergranular phases.

The theoretical volume fractions of equilibrium phases at 170 °C (f_{equ}) in the SiCp/AlCuMgSi and SiCp/2009Al were calculated using Thermo-Calc software. The volume fractions of intragranular precipitates (f) in the DPA SiCp/AlCuMgSi and SiCp/2009Al were calculated based on TEM images. The number density, radius (r) and length of intragranular precipitates were counted according to Fig. 2(a and b).

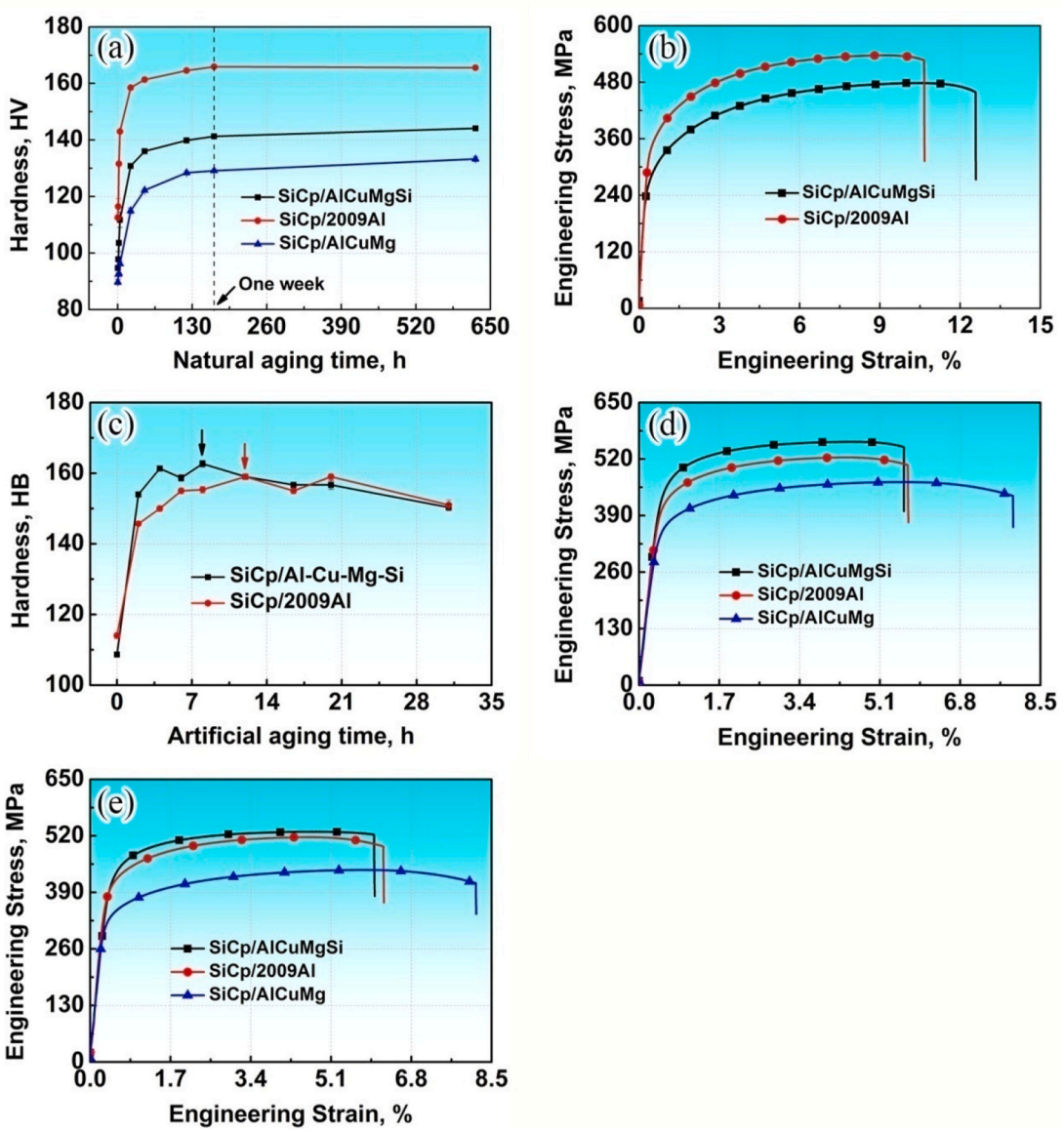

Fig. 1. (a) Variation of hardness of various composites with NA time; (b) engineering stress-strain curves in one-week NA state; (c) variation of hardness of various composites with AA time at 170 °C; (d–e) engineering stress-strain curves in (d) DPA and (e) NPA states.

And thickness of the TEM foil was calculated according to convergent beam electron diffraction images (supplementary data, Fig. S1). The results are listed in Table 2.

The SiCp/AlCuMgSi had a lower f_{equ} than the SiCp/2009Al due to the fewer alloying elements, but f of the two composites was nearly the same. Compared to that in the SiCp/2009Al, the reduction of intergranular phases (Fig. 4) in the SiCp/AlCuMgSi indicates that alloying elements could be transformed into intragranular precipitates in a higher proportion, so the SiCp/AlCuMgSi had equal quantity (volume fraction) of intragranular precipitates compared to the SiCp/2009Al.

4. Discussion

4.1. Mechanisms of reduced NA strength in the SiCp/AlCuMgSi

In the NA state, the difference in YS between the SiCp/AlCuMgSi and SiCp/2009Al was mainly attributed to their different solution strengthening and cluster strengthening (details of the analysis were listed in the supplementary data). Solution strengthening was caused by the obstruction of solute atoms to dislocation movement [10]. During NA, solute atoms can form atom clusters from the supersaturated solid solution. These clusters have strong interaction with dislocations, thereby impeding their movement, that is, cluster strengthening [5]. These two strengthening mechanisms were sensitive to the concentration and feature of solute atoms [5,10].

On the one hand, the content of alloying elements in the SiCp/AlCuMgSi was lower than that in the SiCp/2009Al (Table 1). On the other hand, the radii of Cu atoms and Si atoms are 15% and 6% smaller than Al atoms [23], while their shear moduli are 84% and 50% larger than Al atoms [24,25], respectively, suggesting that Si had smaller atomic size mismatch and shear modulus mismatch with the Al matrix than Cu. Therefore, the SiCp/AlCuMgSi had weaker solution and cluster strengthening than the SiCp/2009Al.

4.2. Mechanisms of increased DPA strength in the SiCp/AlCuMgSi

In the DPA state, YS is dominated by precipitation strengthening, which is controlled by intragranular precipitates radius (r) and volume fractions (f) [26].

Si could refine intragranular precipitates (Fig. 2) and reduce

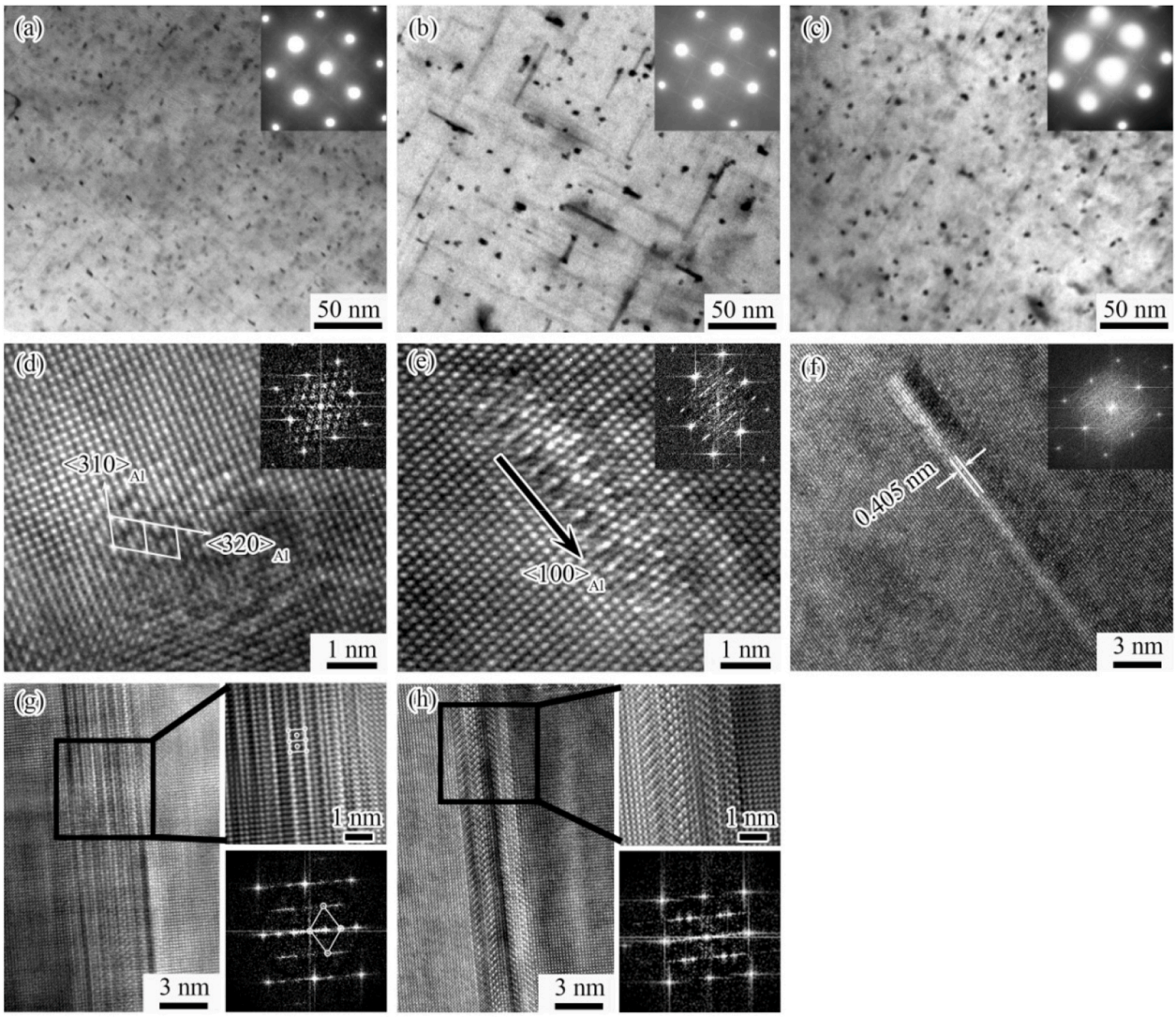

Fig. 2. Characterization of intragranular precipitates in DPA state: (a–c) typical BF and corresponding SAED images of (a)SiCp/AlCuMgSi, (b) SiCp/2009Al and (c) SiCp/AlCuMg; (d–h) HRTEM and corresponding FFT images of SiCp/AlCuMgSi.

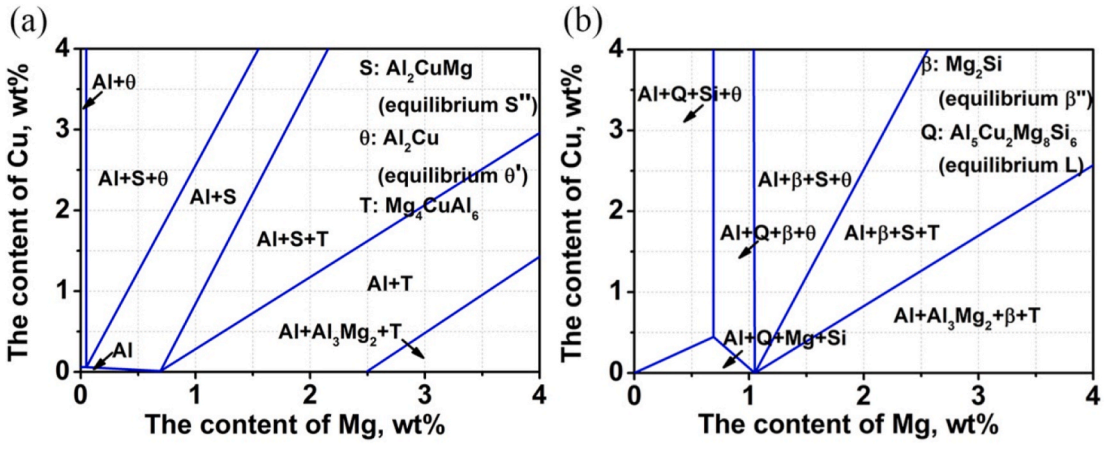

Fig. 3. Aluminum-rich corners of (a) Al–Cu–Mg and (b) Al–Cu–Mg-0.6 wt%Si phase diagrams at 170 °C.

intergranular phases (Fig. 4), so the SiCp/AlCuMgSi had finer and equal quantity (volume fraction) of intragranular precipitates compared to the SiCp/2009Al, leading to the higher DPA strength.

In the SiCp/AlCuMgSi, the refined intragranular precipitates due to Si addition mainly result from the following factors.

During AA, the formation of nano-sized precipitates starts with atom

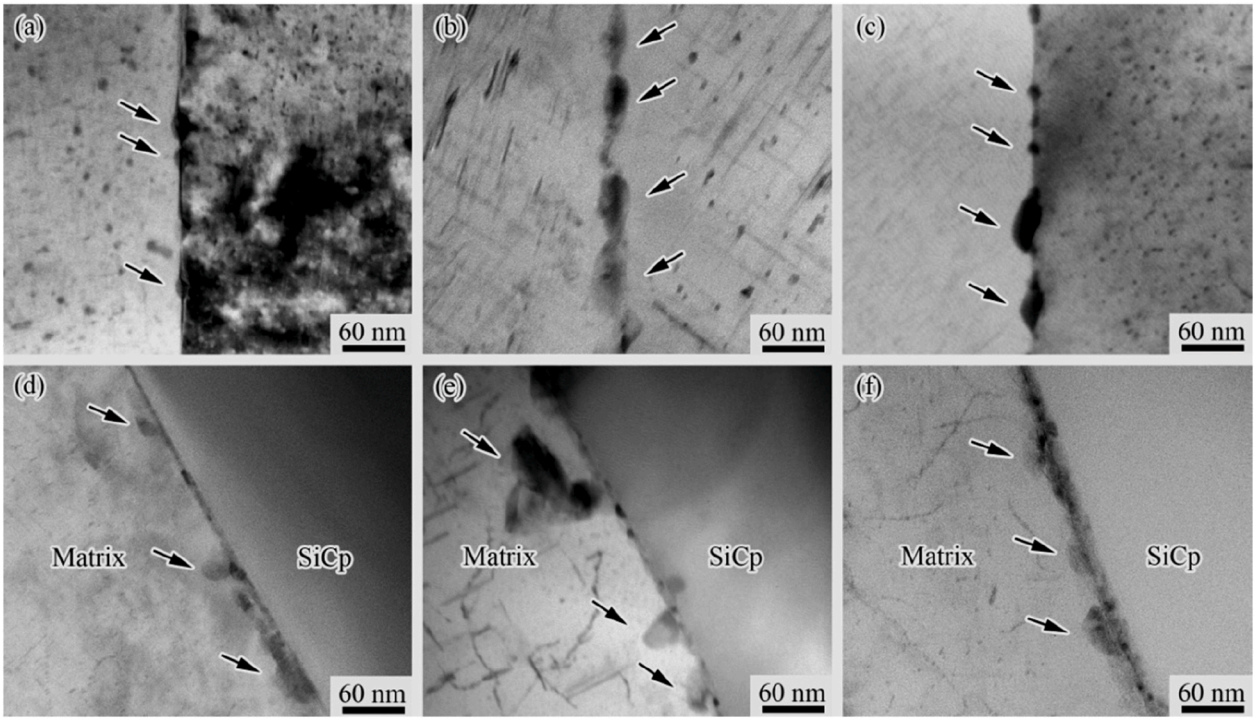

Fig. 4. Typical BF images showing intergranular phases (pointed by arrows) in DPA state at (a–c) grain boundaries and (d–f) interfaces between the SiCp and matrix in (a)(d) SiCp/AlCuMgSi, (b)(e) SiCp/2009Al and (c)(f) SiCp/AlCuMg, respectively.

Table 2
The theoretical volume fractions of equilibrium phases (f_{equ}) and the volume fractions of intragranular precipitates (f) in SiCp/AlCuMgSi and SiCp/2009Al.

Composite designations	f_{equ}, %				f, %
	Mg_2Si	Al_2Cu	Al_2CuMg	Total	
SiCp/AlCuMgSi	2.24	1.90	0.52	4.66	2.02
SiCp/2009Al	/	1.08	5.24	6.32	2.03

clusters [27]. Diffusion coefficients and vacancy interaction energies of solute atoms are important for this procedure [28,29]. In the SiCp/2009Al, Mg-rich clusters are dominant at the initial AA stage because Mg has a high diffusion coefficient and strong interaction with vacancies [30]. In the SiCp/AlCuMgSi, Si is easier to form clusters than Mg due to its faster diffusion and easier interaction with vacancies in the Al matrix [28,29]. Therefore, Si can enrich nucleation sites and enhance nucleation, leading to the finer and denser intragranular precipitates.

In addition, the intragranular precipitates in the DPA SiCp/AlCuMgSi were dominated by GPB zones, β'' and L phases. These zones and phases are much finer than θ′ and S′ phases [21], which are the main intragranular precipitates in the DPA SiCp/2009Al [31]. This is another factor for the refined intragranular precipitates.

In the SiCp/AlCuMgSi, the Si-induced intergranular phase reduction mainly results from the following factors.

Phases at the grain boundaries are mainly formed during AA [32], and are competitive with intragranular precipitates [33]. The enhanced nucleation of intragranular precipitation leads to the decreased phases at grain boundaries.

Phases at the interfaces between SiCp and the matrix are mainly formed during hot pressing and subsequent cooling [2,31,34,35]. Si can reduce phases at interfaces through inhibiting interface chemical reactions because Si is one of the reaction products [31,35–37]. Consequently, the SiCp/AlCuMgSi had fewer phases at interfaces than the SiCp/2009Al although its hot pressing temperature was higher.

5. Conclusions

A strategy was developed to enhance cold plastic forming performance for SiCp/Al composites. According to the strategy, the SiCp/AlCuMgSi, with much lower Cu and slightly added Si compared to the SiCp/2009Al, was designed. Compared to the SiCp/2009Al, the SiCp/AlCuMgSi had a 73 MPa decrement in YS and an increment in uniform elongation from 8.5% to 10.5% after one-week natural aging, but exhibited a 33 MPa increment in YS after AA. The reduced NA strength resulted from the dramatically decreased Cu. The improved AA strength is attributed to the Si-modified precipitation. Si could refine intragranular precipitates and could promote alloying elements to transform into intragranular precipitates. Therefore, compared to the SiCp/2009Al, the SiCp/AlCuMgSi had finer and equal quantity (volume fraction) of intragranular precipitates despite fewer alloying elements.

CRediT authorship contribution statement

S.Z. Zhu: Methodology, Investigation, Visualization, Writing – original draft. **D. Wang:** Data curation, Funding acquisition. **Y.N. Zan:** Investigation. **B.L. Xiao:** Conceptualization, Writing – review & editing, Funding acquisition. **Z.Y. Ma:** Supervision, Writing – review & editing.

Declaration of competing interest

The authors declare that they have no known competing financial interests or personal relationships that could have appeared to influence the work reported in this paper.

Acknowledgments

The authors gratefully acknowledge the support of the National Key R & D Program of China (No. 2017YFB0703104) and the National Natural Science Foundation of China (grant No. 51671191).

Appendix A. Supplementary data

Supplementary data to this article can be found online at https://doi.org/10.1016/j.coco.2021.100742.

References

[1] J.F. Zhang, H. Andrae, X.X. Zhang, Q.Z. Wang, B.L. Xiao, Z.Y. Ma, An enhanced finite element model considering multi strengthening and damage mechanisms in particle reinforced metal matrix composites, Compos. Struct. 226 (2019), https://doi.org/10.1016/j.compstruct.2019.111281.

[2] D. Wang, B.L. Xiao, Q.Z. Wang, Z.Y. Ma, Evolution of the microstructure and strength in the nugget zone of friction stir welded SiCp/Al-Cu-Mg composite, J. Mater. Sci. Technol. 30 (1) (2014) 54–60, https://doi.org/10.1016/j.jmst.2013.09.018.

[3] X.X. Zhang, L.H. Wu, H. Andra, W.M. Gan, M. Hofmann, D. Wang, D.R. Ni, B. L. Xiao, Z.Y. Ma, Effects of welding speed on the multiscale residual stresses in friction stir welded metal matrix composites, J. Mater. Sci. Technol. 35 (5) (2019) 824–832, https://doi.org/10.1016/j.jmst.2018.11.005.

[4] D. Wang, B.L. Xiao, Q.Z. Wang, Z.Y. Ma, Friction stir welding of SiCp/2009Al composite plate, Mater. Des. 47 (2013) 243–247, https://doi.org/10.1016/j.matdes.2012.11.052.

[5] M.J. Starink, N. Gao, L. Davin, J. Yan, A. Cerezo, Room temperature precipitation in quenched Al-Cu-Mg alloys: a model for the reaction kinetics and yield strength development, Philos. Mag. A 85 (13) (2005) 1395–1417, https://doi.org/10.1080/14786430412331333374.

[6] L.F. Mondolfo, Aluminum Alloys: Structure and Properties, Butterworths, London, 1976.

[7] S. Pogatscher, H. Antrekowitsch, M. Werinos, F. Moszner, S.S. Gerstl, M.F. Francis, W.A. Curtin, J.F. Loffler, P.J. Uggowitzer, Diffusion on demand to control precipitation aging: application to Al-Mg-Si alloys, Phys. Rev. Lett. 112 (22) (2014) 225701, https://doi.org/10.1103/PhysRevLett.112.225701.

[8] M. Werinos, H. Antrekowitsch, T. Ebner, R. Prillhofer, W.A. Curtin, P. J. Uggowitzer, S. Pogatscher, Design strategy for controlled natural aging in Al-Mg-Si alloys, Acta Mater. 118 (2016) 296–305, https://doi.org/10.1016/j.actamat.2016.07.048.

[9] F. Lotter, D. Petschke, F. De Geuser, M. Elsayed, G. Sextl, T.E.M. Staab, In situ natural aging of Al-Cu-(Mg) alloys: the effect of in and Sn on the very early stages of decomposition, Scripta Mater. 168 (2019) 104–107, https://doi.org/10.1016/j.scriptamat.2019.04.031.

[10] R.L. Fleischer, Substitutional solution hardening, Acta Metall. 11 (3) (1963) 203–209, https://doi.org/10.1016/0001-6160(63)90213-x.

[11] A.J. Ardell, Precipitation hardening, Metall. Mater. Trans. 16 (12) (1985) 2131–2165, https://doi.org/10.1007/bf02670416.

[12] C.R. Hutchinson, S.P. Ringer, Precipitation processes in Al-Cu-MS alloys microalloyed with Si, Metall. Mater. Trans. 31 (11) (2000) 2721–2733, https://doi.org/10.1007/bf02830331.

[13] S.S. Liang, S.P. Wen, X.L. Wu, H. Huang, K.Y. Gao, Z.R. Nie, The synergetic effect of Si and Sc on the thermal stability of the precipitates in AlCuMg alloy, Mater. Sci. Eng., A 783 (2020), https://doi.org/10.1016/j.msea.2020.139319.

[14] C. Li, G. Sha, B. Gun, J.H. Xia, X.F. Liu, Y.Y. Wu, N. Birbilis, S.P. Ringer, Enhanced age-hardening response of Al-4Mg-1Cu (wt.%) microalloyed with Ag and Si, Scripta Mater. 68 (11) (2013) 857–860, https://doi.org/10.1016/j.scriptamat.2013.02.009.

[15] Z.W. Zhang, Z.Y. Liu, B.L. Xiao, D.R. Ni, Z.Y. Ma, High efficiency dispersal and strengthening of graphene reinforced aluminum alloy composites fabricated by powder metallurgy combined with friction stir processing, Carbon 135 (2018) 215–223, https://doi.org/10.1016/j.carbon.2018.04.029.

[16] J.F. Zhang, X.X. Zhang, Q.Z. Wang, B.L. Xiao, Z.Y. Ma, Simulation of anisotropic load transfer and stress distribution in SiCp/Al composites subjected to tensile loading, Mech. Mater. 122 (2018) 96–103, https://doi.org/10.1016/j.mechmat.2018.04.011.

[17] S.Z. Zhu, G.N. Ma, D. Wang, B.L. Xiao, Z.Y. Ma, Suppressed negative influence of natural aging in SiCp/6092Al composites, Mater. Sci. Eng., A 767 (2019), https://doi.org/10.1016/j.msea.2019.138422.

[18] H.W. Zandbergen, S.J. Andersen, J. Jansen, Structure determination of Mg_5Si_6 particles in Al by dynamic electron diffraction studies, Science 277 (5330) (1997) 1221–1225, https://doi.org/10.1126/science.277.5330.1221.

[19] M. Torsæter, W. Lefebvre, C.D. Marioara, S.J. Andersen, J.C. Walmsley, R. Holmestad, Study of intergrown L and Q′ precipitates in Al-Mg-Si-Cu alloys, Scripta Mater. 64 (9) (2011) 817–820, https://doi.org/10.1016/j.scriptamat.2011.01.008.

[20] C.F. Pan, Y.D. Yang, S.B. Wang, Y.Y. Liu, S.Q. Hu, Z. Wang, P.K. Shen, Atomistic building blocks of one-dimensional Guinier-Preston-Bagaryatsky zones in Al-Cu-Mg alloys, Mater. Des. 187 (2020), https://doi.org/10.1016/j.matdes.2019.108393.

[21] M. Gazizov, C.D. Marioara, J. Friis, S. Wenner, R. Holmestad, R. Kaibyshev, Precipitation behavior in an Al-Cu-Mg-Si alloy during aging, Mater. Sci. Eng., A 767 (2019) 138369, https://doi.org/10.1016/j.msea.2019.138369.

[22] A. Charai, T. Walther, C. Alfonso, A.M. Zahra, C.Y. Zahra, Coexistence of clusters, GPB zones, S``-, S`- and S-phases in an Al-0.9%Cu-1.4%Mg alloy, Acta Mater. 48 (10) (2000) 2751–2764, https://doi.org/10.1016/s1359-6454(99)00422-x.

[23] H.W. King, Quantitative size-factors for metallic solid solutions, J. Mater. Sci. 1 (1) (1966) 79–90, https://doi.org/10.1007/bf00549722.

[24] K. Edalati, D. Akama, A. Nishio, S. Lee, Y. Yonenaga, J.M. Cubero-Sesin, Z. Horita, Influence of dislocation-solute atom interactions and stacking fault energy on grain size of single-phase alloys after severe plastic deformation using high-pressure torsion, Acta Mater. 69 (2014) 68–77, https://doi.org/10.1016/j.actamat.2014.01.036.

[25] J.J. Wortman, R.A. Evans, Youngs modulus shear modulus and Poissons ratio in silicon and germanium, J. Appl. Phys. 36 (1) (1965) 153–156, https://doi.org/10.1063/1.1713863.

[26] A.W. Zhu, E.A. Starke, Strengthening effect of unshearable particles of finite size: a computer experimental study, Acta Mater. 47 (11) (1999) 3263–3269, https://doi.org/10.1016/s1359-6454(99)00179-2.

[27] G. Sha, R.K.W. Marceau, X. Gao, B.C. Muddle, S.P. Ringer, Nanostructure of aluminium alloy 2024: segregation, clustering and precipitation processes, Acta Mater. 59 (4) (2011) 1659–1670, https://doi.org/10.1016/j.actamat.2010.11.033.

[28] Y. Weng, Z. Jia, L. Ding, S. Muraishi, Q. Liu, Clustering behavior during natural aging and artificial aging in Al-Mg-Si alloys with different Ag and Cu addition, Mater. Sci. Eng., A 732 (2018) 273–283, https://doi.org/10.1016/j.msea.2018.07.018.

[29] S. Hirosawa, F. Nakamura, T. Sato, Mater. Sci. Forum 561–565 (2007) 283–286, 10.4028/www.scientific.net/MSF.561-565.283.

[30] B.P. Huang, Z.Q. Zheng, Independent and combined roles of trace Mg and Ag additions in properties precipitation process and precipitation kinetics of Al-Cu-Li-(Mg)-(Ag)-Zr-Ti alloys, Acta Mater. 46 (12) (1998) 4381–4393, https://doi.org/10.1016/s1359-6454(98)00079-2.

[31] P. Rodrigo, P. Poza, V. Utrilla, A. Urena, Effect of reinforcement geometry on precipitation kinetics of powder metallurgy AA2009/SiC composites, J. Alloys Compd. 479 (1–2) (2009) 451–456, https://doi.org/10.1016/j.jallcom.2008.12.114.

[32] S. Hirosawa, Y. Oguri, T. Sato, Experimental and computational investigation of formation of precipitate free zones in an Al-Cu alloy, Mater. Trans. 46 (6) (2005) 1230–1234, https://doi.org/10.2320/matertrans.46.1230.

[33] C.A. Gandin, A. Jacot, Modeling of precipitate-free zone formed upon homogenization in a multi-component alloy, Acta Mater. 55 (7) (2007) 2539–2553, https://doi.org/10.1016/j.actamat.2006.11.047.

[34] G.N. Ma, D. Wang, Z.Y. Liu, B.L. Xiao, Z.Y. Ma, An investigation on particle weakening in T6-treated SiC/Al-Zn-Mg-Cu composites, Mater. Char. 158 (2019), https://doi.org/10.1016/j.matchar.2019.109966.

[35] J.C. Lee, J.Y. Byun, C.S. Oh, H.K. Seok, H.I. Lee, Effect of various processing methods on the interfacial reactions in SiCp 2024 Al composites, Acta Mater. 45 (12) (1997) 5303–5315, https://doi.org/10.1016/s1359-6454(97)84851-3.

[36] S.Z. Zhu, D. Wang, B.L. Xiao, Z.Y. Ma, Suppressed negative effects of natural aging by pre-aging in SiCp/6092Al composites, Compos. B Eng. 212 (2021) 108730, https://doi.org/10.1016/j.compositesb.2021.108730.

[37] F. Qiu, H. Tong, P. Shen, X. Cong, Y. Wang, Q. Jiang, Overview: SiC/Al interface reaction and interface structure evolution mechanism, Acta Metall. Sin. 55 (1) (2019) 87–100, https://doi.org/10.11900/0412.1961.2018.00292.